ISSN 0965-545X, Polymer Science, Series A, 2019, Vol. 61, No. 4, pp. 514–519. © Pleiades Publishing, Ltd., 2019.
Russian Text © The Author(s), 2019, published in Vysokomolekulyarnye Soedineniya, Seriya A, 2019, Vol. 61, No. 4, pp. 359–365.

THEORY AND SIMULATION

Phase Diagram of Rod-Coil Diblock Copolymers: Dissipative Particle Dynamics Simulation

A. V. Berezkin[a,b,*], Y. V. Kudryavtsev[a,c], and M. A. Osipov[a,d]

[a] *Topchiev Institute of Petrochemical Synthesis, Russian Academy of Sciences Moscow, 119991 Russia*
[b] *Technische Universität München, Garching, 85747 Germany*
[c] *Frumkin Institute of Physical Chemistry and Electrochemistry, Russian Academy of Sciences, Moscow, 119071 Russia*
[d] *University of Strathclyde, Mathematics and Statistics, Glasgow, G1 1XH Scotland, United Kingdom*
** e-mail: berezkin.anatoly1@gmail.com*

Received March 9, 2019; revised March 13, 2019; accepted March 18, 2019

Abstract—Using dissipative particle dynamics, a refined phase diagram of the rod-coil diblock copolymer is constructed in coordinates copolymer composition–repulsion parameter of different types of units. The diagram describes the microphase separation of copolymer blocks and the orientational ordering of rigid blocks. Simulation of rodlike blocks as rigid bodies makes it possible to reduce computational costs, increase the size of the simulation cell to $32 \times 32 \times 32$ and the total length of the copolymer chain N to 20, to vary the composition of the copolymer chain with a smaller step (up to 0.05), and to investigate the behavior of systems with high degrees of segregation of blocks (up to $\chi N \approx 250$). Owing to this optimization, the ordering of rigid blocks not only in the lamellar but also in bicontinuous morphology can be observed for the first time. It is also shown that the zigzag and bilayer lamellas described not only in numerical but also in laboratory experiments are metastable and disappear with an increase in the size of the simulated system.

DOI: 10.1134/S0965545X19040023

INTRODUCTION

Conducting polymers typically have increased rigidity because of the presence of conjugated bonds. One of the ways to improve their solubility, and, as a result, processability, is to use rod-coil block copolymers. Owing to the conformational asymmetry, such copolymers form various microdomain structures used in photovoltaics and related areas [1, 2]. In flexible copolymers, microphase separation is controlled by the ratio of lengths of chemically different blocks and the degree of their segregation. Replacing one of the flexible blocks with a rigid one reduces the conformational entropy of the copolymer, facilitating the emergence of stable microstructures. The aspect ratio of the rod-shaped block becomes an additional factor determining the pattern of the phase diagram. The appearance of a mesogenic fragment in the copolymer enables transition from an isotropic to nematic or smectic ordering of rods in domains.

To date, for rod-coil diblock copolymers, along with conventional morphologies (micelles, cylinders, bicontinuous structures, lamellas), smectic layers [3–7], arrowhead, z-shaped, wavy, and perforated lamellas have been observed [8–24]. For copolymers with semirigid rods, the existence of single- and double-layer lamellas as smectics A and C and various transitions between them was predicted in the framework of the self-consistent mean field theory (SCFT) [22].

The initial theoretical efforts to construct the phase diagram of rod-coil copolymers were aimed at comparing the free energy values for different morphologies [25, 26]. Under the assumption that the rods form smectic A, the formation of micelles in the shape of a hockey puck or hexagonally packed cylinders with a lamellar core of a rectangular cross section consisting of rods was predicted. Further mesoscopic molecular simulation studies [16–18, 23, 24] showed that, in terms of entropy, smectic C is often more favorable than smectic A, since the slope of rods in smectic lamellas is statistically more probable. In addition, in this case, the density of the junction points of flexible and rigid blocks on the surface of lamellas decreases and the conformational entropy of flexible blocks increases.

Subsequently, the construction of the phase diagram of rod-coil copolymers was carried out mainly by SCFT [19–22, 27–31] and molecular dynamics [16–18, 23, 24, 32]. In [18], phase diagrams in coordinates composition–segregation of blocks were systematically investigated by the Brownian molecular dynamics with Lennard-Jones potentials for three fixed values of the length of a rigid block. In this case, various nontrivial morphologies, such as lamellar crystalline,

arrowhead, alternating arrowhead, hexatic B, smectics A and C, lamellar nematic, lamellar, lamellar hexagonal perforated, lamellar wavy, and cylindrical hexagonal, were observed.

The microphase separation of rod-coil copolymers by dissipative particle dynamics (DPD) was studied for the first time by AlSunaidi et al. [23, 24]. Varying the temperature and degree of segregation of the blocks of copolymer R_7C_7 at a particle density of $\rho_0 = 4$, the authors observed the formation of crystalline and smectic A phases. Using DPD, the phase diagram was constructed with a density of $\rho_0 = 5$, the length of the copolymer $N = 10$, and the variable composition of the copolymer and the degree of segregation of its blocks [32]. Crystalline lamellar, lamellar, gyroid, cylindrical, and micellar phases were detected. It should be noted that, owing to the limited length of chains, the composition of the copolymer was varied with a large step ($\Delta f_A = 0.1$). The orientational ordering of chains was observed only at the fraction of the rigid block $f_A \geq 0.7$, when the rigid fragment contained seven or more units. On the whole, DPD leads to phase diagrams close to those obtained by the Brownian molecular dynamics.

To date, the DPD method has been little used to study the phase behavior of rod-coil copolymers. The reason is that the simulation was carried out at a high density of particles, which did not make it possible to consider cells larger than $20 \times 20 \times 20$ and copolymers consisting of more than $N = 10$ units. Relatively short rigid blocks in such molecules had a relatively low tendency toward orientational ordering, and it could only be observed in the lamellar morphology.

In the present work, a more detailed phase diagram of the rod-coil diblock copolymer for chains of length $N = 20$ in a $32 \times 32 \times 32$ cell with an average particle density of $\rho_0 = 3$ was constructed. Because of a greater chain length, the composition of the copolymer in the phase diagram was varied in increments $\Delta f_A = 0.05$ and the maximum investigated degree of segregation χN_{max} reached ≈ 250 (in [32], $\Delta f_A = 0.1$ and $\chi N_{max} = 80$). According to our diagram, orientational ordering can arise not only in the lamellar but also in the bicontinuous morphology.

MODEL AND CALCULATION METHOD

Large-scale molecular simulation of copolymers containing rigid moieties is a challenge [33]. Such systems relax much more slowly than flexible molecular chains of the same length with a wide spectrum of relaxation times, including fast modes of individual units. Among coarsened mesoscopic methods, dissipative particle dynamics is considered one of the most promising. Owing to a large step of integration of the equations of motion and low coefficients of friction of particles with "soft" potentials, this technique makes it possible to observe self-organization of macromolecules on relatively large space-time scales. DPD has already been used to study mixtures of monodisperse [34, 35], bidisperse [36], and diblock rigid nanorods [37] with diblock copolymers that form lamellar [34, 36, 37] and hexagonal [35–37] microdomain structures and to investigate the behavior of carbon nanotubes in a concentrated diblock copolymer solution [38]. The "standard" approach developed by R.D. Groot and P.B. Warren [39] for flexible-chain polymers is not sufficient for simulating rigid blocks. To this end, a number of DPD modifications were proposed for the introduction of rigidity. One of the methods involves the adjustment of valence potentials and the addition of angular potentials [40–46], but it requires reducing the integration step by 5 to 10 times to maintain the stability of the numerical solution of the equations of motion of particles, which slows down calculations. We use an alternative approach, which was shown to be efficient, namely, in simulating rodlike fragments as rigid bodies in the NVE ensemble according to the algorithm of T.F. Miller et al. [47]. It excludes the interaction of particles inside a rigid block from consideration, optimizing the calculation of forces.

Another problem with the standard DPD method is that the nematic ordering of nanorods related to their steric repulsion is difficult. The reason for this is the "softness" of interparticle interactions compared to classical molecular potentials, such as the Lennard-Jones potential. To overcome these difficulties, various approaches were developed. In [40–43], the length of bonds in the rigid block was halved, which led to an increase in density and the corresponding strengthening of steric interactions. Unfortunately, the number of particles and, consequently, the computational cost equally increased. According to the literature, the nematic ordering of rigid [23] and semirigid [48] rods using standard DPD potentials can be observed only at the length of the rigid rod $N_R \geq 7$. In this paper, simulations were performed using both the repulsion parameter of identical particles $a_{AA} = a_{BB} = 25$, which is usual for DPD, and $a_{AA} = a_{BB} = 50$. This facilitates the orientational ordering of rodlike particles. However, the effect of the repulsion parameter was relatively weak; therefore, the main results are given for the standard case.

A more detailed description of DPD can be found, for example, in our recent work [49] devoted to the statistical thermodynamics of flexible-chain diblock copolymers doped with nanorods. For calculations, the LAMMPS software package was used.

RESULTS AND DISCUSSION

Microphase separation in a block copolymer with a variable ratio of the lengths of rigid A and flexible B blocks and constant total chain length $N = 20$ was simulated by means of a gradual (with a step of 0.1)

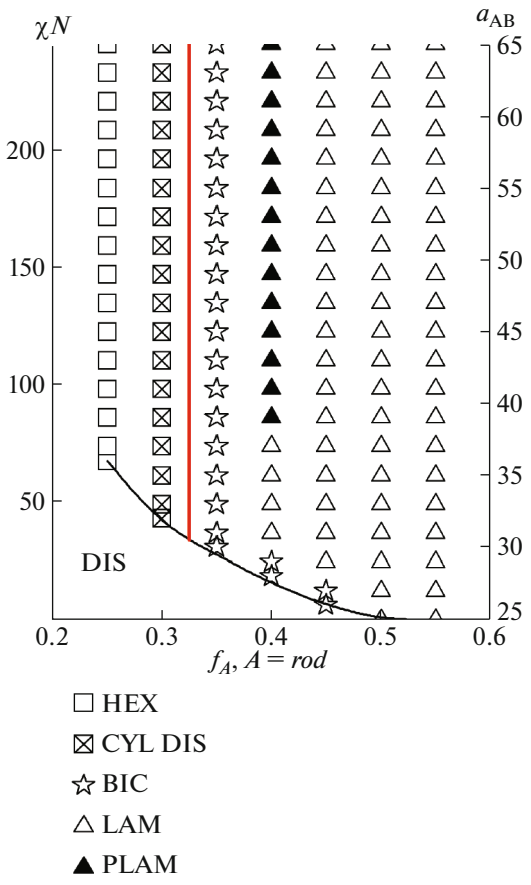

Fig. 1. (Color online) Rod-coil diblock copolymer phase diagram in coordinates $\chi N - f_A$ (or $a_{AB} - f_A$) at $a_{AA} = a_{BB} = 25$. Morphology: DIS is the disordered homogeneous melt, HEX is hexagonally packed cylindrical domains, CYL DIS is disordered cylinders or long micelles, BIC is the bicontinuous morphology, PLAM is perforated lamellas, and LAM is lamellas.

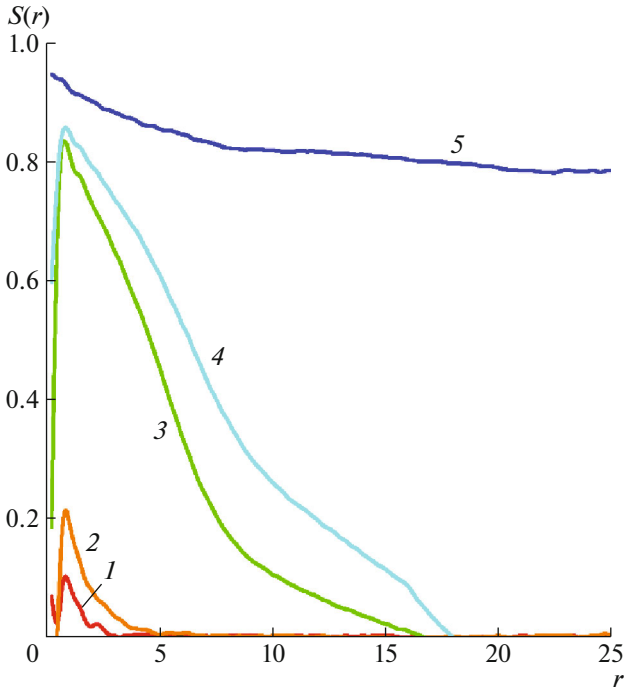

Fig. 2. (Color online) Correlation function $S_N(r)$ of orientation of bonds in rigid blocks A of copolymer A_8B_{12} with the degree of segregation of rigid and flexible blocks a_{AB} = (*1*) 25 (DIS), (*2*) 27 (DIS), (*3*) 29 (BIC), (*4*) 31 (BIC), and (*5*) 33 (LAM). At $a_{AB} = 27.5$, microphase separation occurs to form the bicontinuous structure; at $a_{AB} = 30$, the lamellar structure.

increase in the repulsion parameter a_{AB} between particles of different types for the initially disordered state. This value is related to the Flory–Huggins parameter χ via linear relationship $\chi = (0.306 \pm 0.003)(a_{AB} - a_{AA})$ [39]. Simulations were carried out in a $32 \times 32 \times 32$ cell, where the cut-off radius of interactions between DPD particles was taken as a unit of length.

Different microstructures in the system were identified by the appearance of secondary peaks on the dependence of the static structure factor of the rigid block on the wave vector [50]. Orientational ordering was detected visually, and to quantify it, the value of the correlation function $S_N(r)$ was calculated depending on distance r between bonds A–A in rods:

$$S_N(r) = \left\langle \frac{1}{2}[3(\mathbf{n}_i \cdot \mathbf{n}_j)^2 - 1] \right\rangle,$$

where angle brackets mean averaging over 10^5 randomly selected pairs of A–A bonds belonging to different rods with unit vectors $\mathbf{n}_i$ and $\mathbf{n}_j$. In the absence of the long-range orientational order, $S_N \to 0$ at $r \to \infty$, but in the perfect nematic, $S_N = 1$.

Figure 1 shows the phase diagram of the AB rod-coil diblock copolymer constructed in coordinates $\chi N - f_A$ (molar fraction of units A in the copolymer) for $a_{AA} = a_{BB} = 25$. From the point of view of microphase separation, the diagram is morphologically similar to the phase diagram of a flexible-chain diblock copolymer constructed using the DPD technique [50]. The degree of segregation of units A and B corresponding to the disorder–order transition depends on the composition of the copolymer and increases with decreasing length of the rigid block.

At $f_A > 0.3$ ($N_A > 6$), orientational ordering is observed in the domains formed by rigid blocks. The corresponding area of the diagram in Fig. 1 is located to the right of the solid vertical line.

The behavior of the orientational correlation function $S_N(r)$ for copolymer A_8B_{12} at different segregation strength of the units of blocks A and B is shown in Fig. 2. In the case of weak incompatibility ($a_{AB} = 25$ and 27), ordering appears only at distances less than the length of the rod. However, with increasing distance a_{AB}, at which S_N is nonzero (the correlation length of the orientational interaction of rods), ordering increases markedly. For $a_{AB} = 29$ and 31, this dis-

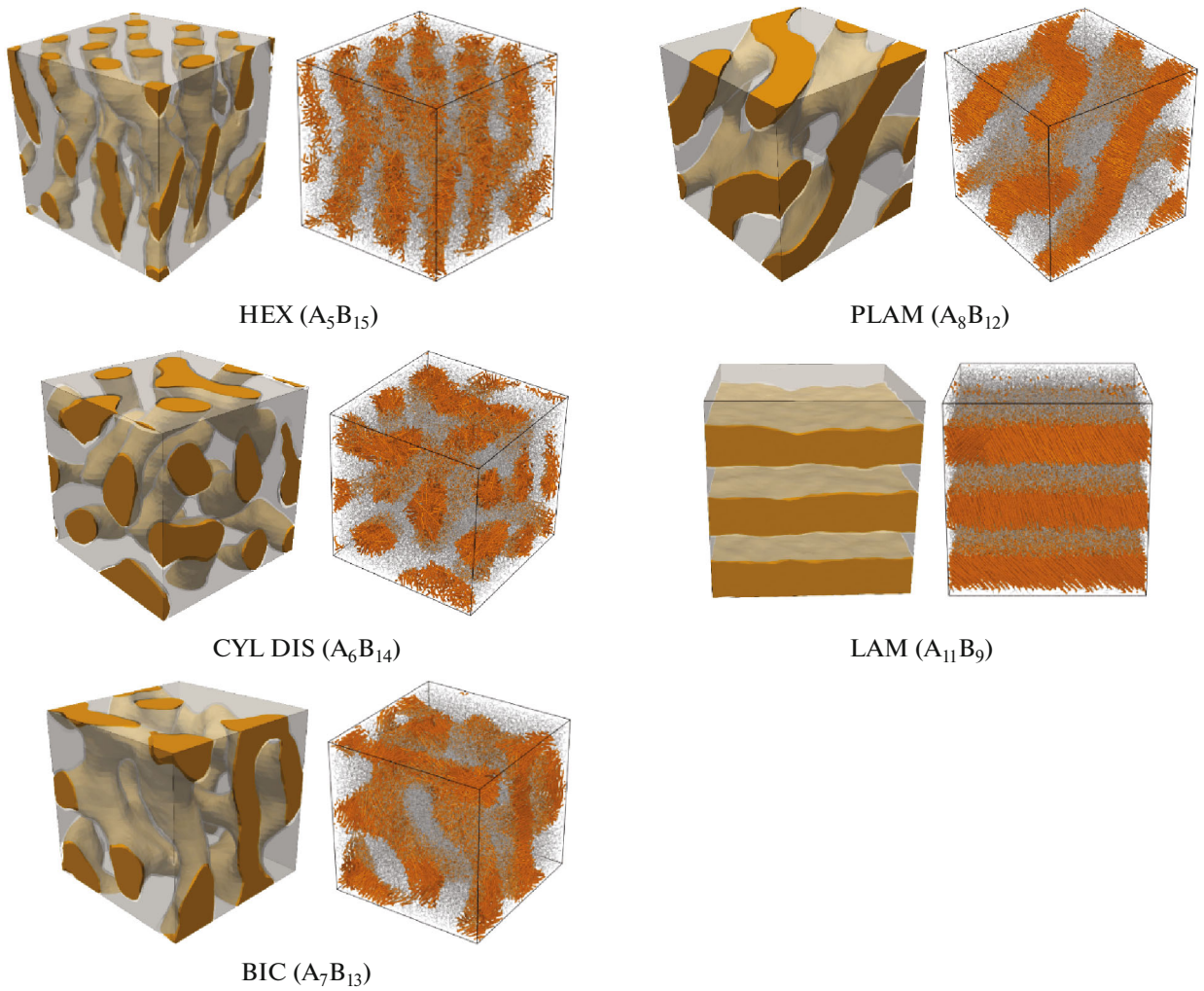

Fig. 3. (Color online) Instant snapshots of rod-coil copolymers in various ordered states. The structure of the interface area is shown on the left, and the location of rigid (yellow) and flexible (gray) copolymer blocks is shown on the right. Color drawings can be viewed in the electronic version of the journal.

tance is comparable to the size of the domains and, when a lamellar microstructure ($a_{AB} = 33$) is formed, it exceeds the size of the simulation cell. This indicates the occurrence of long-range order in the arrangement of rigid blocks.

The structure of the emerging morphologies is shown in Fig. 3. In copolymer A_5B_{15} with a short rigid block, hexagonally ordered cylinders (HEX) are formed. Lengthening of the rigid block leads to the disordering of cylinders (CYL DIS) for copolymer A_6B_{14} and bicontinuous morphology (BIC) for A_7B_{13}. In copolymer A_8B_{12}, lamellas (LAM) are formed, which are also stable in copolymers with a longer rigid block A. A regular bicontinuous structure similar to perforated lamellas (PLAM) was also found. It is not yet clear whether this structure is kinetically stable.

The transition from the isotropic to ordered distribution of rigid blocks is observed only in the microphase-separated state of the copolymer. In contrast to the results of [32], this state does not necessarily correspond to the lamellar morphology. In this case, only smectic C appears, in which a decrease in the density of chains per unit interface area, which increases the conformational entropy of flexible blocks, is achieved by tilting the rods in the lamellas. As follows from Fig. 3, the direction of the director of the smectic phase changes from one lamella to another.

In the future, it will be of interest to construct a phase diagram in coordinates $\chi N - f_A$ at $N_A = 7$ or 8, varying the length of the flexible block and the full length of the copolymer chain, since rigid blocks of such a length are always orientationally ordered.

Figure 4 shows the phase diagram and snapshots of ordered states similar to those shown in Figs. 1 and 3 but corresponding to a stronger repulsion of identical units: $a_{AA} = a_{BB} = 50$. It is seen that, on one hand, an increase in the steric repulsion of DPD particles facil-

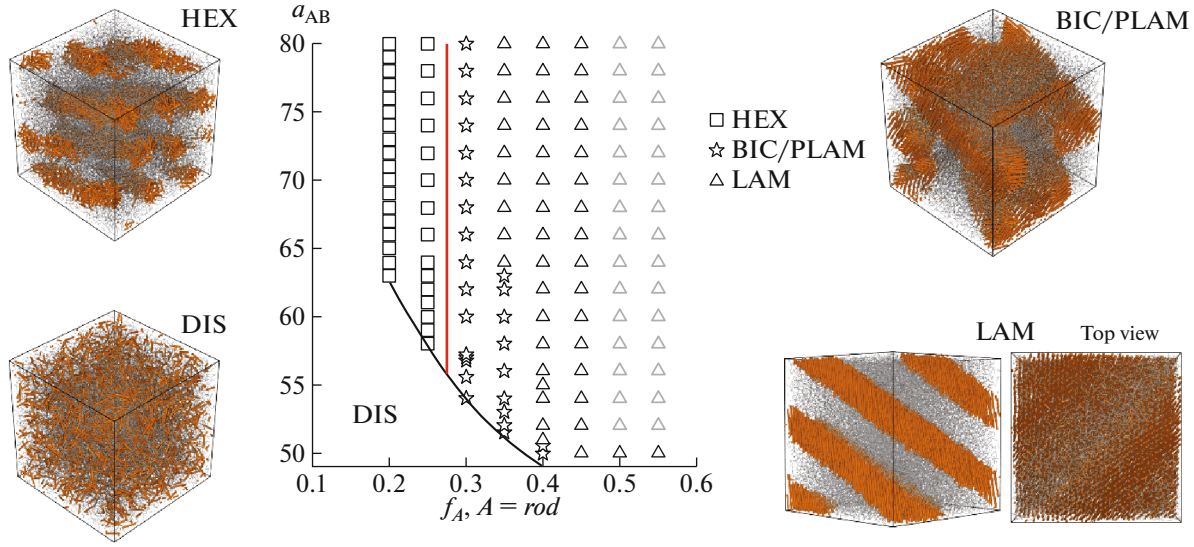

Fig. 4. (Color online) The rod-coil diblock copolymer phase diagram and instant snapshots of various morphologies at $a_{AA} = a_{BB} = 50$. The hexagonal packing of rigid blocks is shown by the example of the lamellar structure.

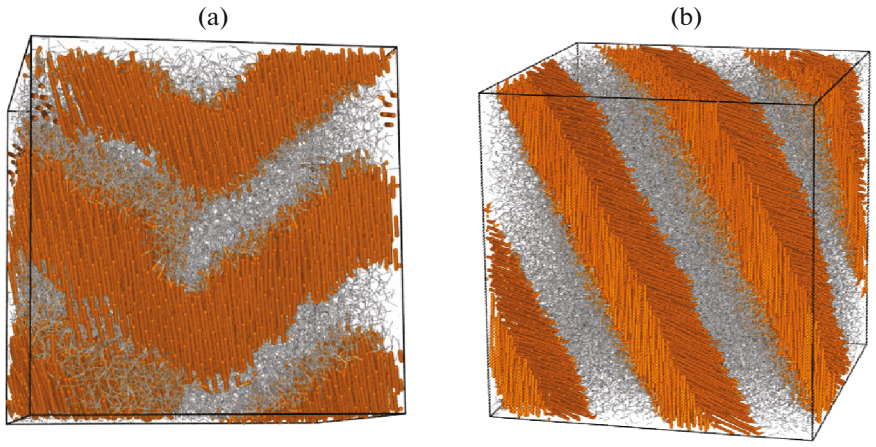

Fig. 5. (Color online) Metastable morphologies arising in a cell of size 20 × 20 × 20: (a) zigzag lamellas ($N_A = 10$, $a_{AA} = a_{BB} = a_{AB} = 50$) and (b) disordered double-layer lamellas ($N_A = 11$, $a_{AA} = a_{BB} = 25$, $a_{AB} = 50$).

itates the orientational ordering of rods which appear at $N_A = 6$. On the other hand, the viscosity of the system and its relaxation time increase significantly. At $N_A = 8$, no noticeable morphology rearrangements are observed at times on the order of 10^7 integration steps, and at $N_A \geq 10$, the relaxation of microdomain structure defects in a reasonable time is impossible. At $N_A > 8$, rigid blocks form a structure that is close to a crystal in the degree of order.

In separate numerical experiments conducted in cells of a smaller size (20 × 20 × 20), exotic structures appeared, namely, zigzag lamellas with $N_A = 10$ and disordered fragments of double-layer lamellas with $N_A = 11$. They are shown in Fig. 5. The resimulation in 32 × 32 × 32 cells demonstrated that these morphologies are metastable and not reproduced, giving way to flat single-layer lamellas.

Thus, in further DPD simulations of rod-coil copolymers, it seems more reasonable to use the standard value of the repulsion parameter $a_{AA} = a_{BB} = 25$ and to verify the stability of arising morphologies in larger cells.

The refined rod-coil diblock copolymer phase diagram can be used to interpret laboratory experiments and compare them with theoretical calculations.

FUNDING

This work was supported by the Russian Science Foundation (project 16-13-10280).

ACKNOWLEDGMENTS

A.V. Berezkin is grateful for the opportunity to use the equipment of the Center for Collective Use of Superhigh-Performance Computing Resources, Lomonosov Moscow State University.

REFERENCES

1. M. He, F. Qiu, and Z. Lin, J. Mater. Chem. **21**, 17039 (2011).
2. Y. Lee and E. D. Gomez, Macromolecules **48**, 7385 (2015).
3. M. Lee, B.-K. Cho, H. Kim, and W.-C. Zin, Angew. Chem., Int. Ed. **37**, 638 (1998).
4. M. Lee, B.-K. Cho, H. Kim, J.-Y. Yoon, and W.-C. Zin, J. Am. Chem. Soc. **120**, 9168 (1998).
5. J.-H. Ryu and M. Lee, Struct. Bonding (Berlin, Germ.) **128**, 63 (2008).
6. B. D. Olsen and R. A. Segalman, Macromolecules **39**, 7078 (2006).
7. L. R. N. Sary, C. Brochon, G. Hadziioannou, J. Ruokolainen, and R. Mazzenga, Macromolecules **40**, 6990 (2007).
8. L. H. Radzilowski, J. L. Wu, and S. I. Stupp, Macromolecules **26**, 879 (1993).
9. L. H. Radzilowski and S. I. Stupp, Macromolecules **27**, 7747 (1994).
10. L. H. Radzilowski, B. O. Carragher, and S. I. Stupp, Macromolecules **30**, 2110 (1997).
11. J. T. Chen, E. L. Thomas, C. K. Ober, and S. S. Hwang, Macromolecules **28**, 1688 (1995).
12. J. T. Chen, E. L. Thomas, C. K. Ober, and G. O. Mao, Science **273** (5273), 343 (1996).
13. J.-H. Ryu, N.-K. Oh, W.-C. Zin, and M. J. Lee, J. Am. Chem. Soc. **126**, 3551 (2004).
14. S. A. Jenekhe and X. L. Chen, Science **279** (5358), 1903 (1998).
15. M. Lee, B.-K. Cho, K. J. Ihn, W.-K. Lee, N.-K. Oh, and W.-C. Zin, J. Am. Chem. Soc. **123**, 4647 (2001).
16. M. A. Horsch, Z. L. Zhang, and S. C. Glotzer, Phys. Rev. Lett. **95**, 056105 (2005).
17. M. A. Horsch, Z. L. Zhang, and S. C. Glotzer, J. Chem. Phys. **125**, 184903 (2006).
18. M. A. Horsch, Z. L. Zhang, and S. C. Glotzer, Soft Matter **6**, 945 (2010).
19. J. Z. Chen, C. X. Zhang, Z. Y. Sun, Y. S. Zheng, and L. J. An, J. Chem. Phys. **124**, 104907 (2006).
20. J. Z. Chen, C. X. Zhang, Z. Y. Sun, L. J. An, and Z. J. Tong, J. Chem. Phys. **127**, 024105 (2007).
21. J. Z. Chen, Z. Y. Sun, C. X. Zhang, L. J. An, and Z. J. Tong, J. Chem. Phys. **128**, 074904 (2008).
22. W. D. Song, P. Tang, F. Qiu, Y. L. Yang, and A. C. Shi, Soft Matter **7**, 929 (2011).
23. A. AlSunaidi, W. K. den Otter, and J. H. R. Clarke, Philos. Trans. R. Soc. London **362** (1821), 1773 (2004).
24. A. AlSunaidi, W. K. den Otter, and J. H. R. Clarke, J. Chem. Phys. **130**, 124910 (2009).
25. A. Halperin, Macromolecules **23**, 2724 (1990).
26. D. R. M. Williams and G. H. Fredrickson, Macromolecules **25**, 3561 (1992).
27. M. Müller and M. Schick, Macromolecules **29**, 8900 (1996).
28. M. W. Matsen and C. Barrett, J. Chem. Phys. **109**, 4108 (1998).
29. V. Pryamitsyn and V. Ganesan, J. Chem. Phys. **120**, 5824 (2004).
30. M. Shah, V. Pryamitsyn, and V. Ganesan, Macromolecules **41**, 218 (2008).
31. Yu. A. Kriksin and P. G. Khalatur, Macromol. Theory Simul. **21**, 382 (2012).
32. L. He, Z. Chen, R. Zhang, L. Zhang, and Zh. Jiang, J. Chem. Phys. **138**, 094907 (2013).
33. L.-T. Yan and X.-M. Xie, Prog. Polym. Sci. **38**, 369 (2013).
34. L. He, L. Zhang, A. Xia, and H. Liang, J. Chem. Phys. **130**, 144907 (2009).
35. L. He, L. Zhang, H. Chen, and H. Liang, Polymer **50**, 3403 (2009).
36. L. He, L. Zhang, and H. Liang, Polymer **51**, 3303 (2010).
37. A. Chai, D. Zhang, Y. Jiang, L. He, and L. Zhang, J. Chem. Phys. **139**, 104901 (2013).
38. Z. Zhang, T. Li, and E. Nies, Macromolecules **47**, 5416 (2014).
39. R. D. Groot and P. B. Warren, J. Chem. Phys. **107**, 4423 (1997).
40. S.-H. Chou, H.-K. Tsao, and Y.-J. Sheng, J. Chem. Phys. **134**, 034904 (2011).
41. S.-H. Chou, D. T. Wu, H.-K. Tsao, and Y.-J. Sheng, Soft Matter **7**, 9119 (2011).
42. O. Liba, D. Kauzlaric, Z. R. Abrams, Y. Hanein, A. Greiner, and J. G. Korvink, Mol. Simul. **34**, 737 (2008).
43. Ch. Zhou, S.-K. Luo, Y. Sun, Y. Zhou, and W. Qian, J. Appl. Polym. Sci. **133**, 44098 (2016).
44. Y. K. Levine, A. E. Gomes, A. F. Martins, and A. Polimeno, J. Chem. Phys. **122**, 144902 (2005).
45. Z. Zhang and H. Guo, J. Chem. Phys. **133**, 144911 (2010).
46. X. Li, F. Huang, T. Jiang, X. He, S. Lin, and J. Lin, RSC Adv. **5**, 1514 (2015).
47. T. F. Miller, M. Eleftheriou, P. Pattnaik, A. Ndirango, D. Newns, and G. J. Martyna, J. Chem. Phys. **116**, 8649 (2002).
48. A. Polimeno, A. Gomes, and A. F. Martins, in *Computer Simulation of Liquid Crystals and Polymers, NATO Science Series II,* Ed. by P. Pasini, C. Zannoni, and S. Žumer (Kluwer, Dordrecht, 2005), Vol. 177.
49. A. V. Berezkin, Y. V. Kudryavtsev, M. V. Gorkunov, and M. A. Osipov, J. Chem. Phys. **146**, 144902 (2017).
50. A. A. Gavrilov, Y. V. Kudryavtsev, and A. V. Chertovich, J. Chem. Phys. **139**, 224901 (2013).